JOURNAL OF SOLID STATE CHEMISTRY 119, 36–44 (1995)

FT-IR Skeletal Study of $RBa_2Cu_3O_{7-y}$ (R = Ln or Y) and $Nd_{2-x}Ce_xCuO_4$ Cuprate Powders

Marco Daturi,* Guido Busca,* Edoardo Magnone,† and Maurizio Ferretti†

*Istituto di Chimica, Facoltà di Ingegneria, Università, P.le Kennedy, I-16129 Genova, Italy; and †Istituto di Chimica Fisica, Facoltà di Scienze M.F.N., Università, C.so Europa 26, I-16132 Genova, Italy

Received December 6, 1994; in revised form March 10, 1995; accepted March 15, 1995

The FT-IR/FT-FIR spectra of powders of $Nd_{2-x}Ce_xCuO_4$ solid solutions ($x \leq 0.25$) and of $RBa_2Cu_3O_{7-y}$ ($y = 0.2$–0.3) with R = Y, Pr, Nd, Sm, Eu, Gd, Dy, Ho, Er, Tm, and Yb, have been recorded at room temperature. A comparison with the published single crystal IR data is made. An empirical assignment of the observed bands is proposed on the basis of the factor group analysis and a discussion of the internal vibrational structure of the CuO_x structures is given. © 1995 Academic Press, Inc.

1. INTRODUCTION

Besides $La_{2-x}Sr_xCuO_4$ (1), several other cuprate families have been shown to act as superconductors at relatively high temperature (15 K $\leq T_c \leq$ 130 K). All these families contain nearly planar sheets of square-coordinated copper ions and linearly bridging oxygen atoms $[CuO_2]_n$, although they differ in the multiplicity of such sheets and the nature of the blocks that separate them and, finally, in the presence of additional $[CuO_3]_m$ chains and the total coordination at copper (square-planar, square-pyramidal, or bipyramidal) (2, 3).

Vibrational spectroscopies have been largely utilized for the characterization of these materials and give valuable information on the phonon modes, on their coupling with electronic excitation, and on the superconducting gap in such structures (4). The factor group analyses for the most studied structures have also been performed (4, 5). However, although a very large number of Raman studies of cuprates have been published (5, 6), literature infrared studies are relatively few and somewhat incomplete. The data arising from vibrational spectroscopies, mainly using single crystal measurements have been the basis of lattice dynamics calculations that allowed one to propose models for the atom motions upon the fundamental vibrational modes (4–6). However, fit of the calculated frequency values with the experimental ones is not always good, and calculations performed by different groups give rather scattered data (4–7). On the other hand, the vibrational spectra of superconductor powders have been discussed in lesser detail, and comparison of the vibrational spectra of different cuprate systems, in spite of their potential interest, seems also to be lacking. To allow such comparative studies, band assignments to well-defined vibrational modes of structural subunits of the different crystal structures are helpful. For this reason, spectra interpretation based on group approximation could be useful, in spite of the fact that the lattice dynamics calculations show that they are more or less unrealistic.

Following previous researches on cuprate superconductors (8, 9) and on lattice vibrations of solids (10, 11), we undertook a characterization of some of these phases in the form of powders by far infrared spectroscopy. We present here a discussion of the powder IR spectra of some of these materials belonging to the so-called 214 system $Nd_{2-x}Ce_xCuO_4$ (NCCO) and 123 system $RBa_2Cu_3O_{7-x}$ (RBCO) and give an empirical assignment of the vibrational modes.

2. EXPERIMENTAL

The cuprate samples have been prepared via solid state reaction using stoichiometric amounts of the precursor oxides. For the 214 $Nd_{2-x}Ce_xCuO_4$ (NCCO) solid solutions Nd_2O_3, CeO_2 and CuO powders have been calcined at 1373 K, according to the previously determined phase diagram (12). For the 123 RBCO samples the oxides of R = Y, Pr, Nd, Sm, Eu, Gd, Dy, Ho, Er, Tm, and Yb have been heated together with CuO and BaO_2. In this case, the thermal program is constituted by a heating rate of 200°C/hr, an isothermal stop at 900°C $< T <$ 950°C (depending upon the thermodynamics of each system), and a cooling rate at 200°C/hr. All powders have been mixed in a Mettler agatha miller, using ethyl alcohol as emulsifying agent. The mixtures have been subsequently submitted to thermal treatments in an electronic controlled Carbolite furnace.

Phase recognition has been performed by XRD analysis in a Philips 1710 X-ray powder diffractometer. The thermodynamics of the samples has been investigated by a TG–DTA Netzsch apparatus.

0022-4596/95 $12.00

TABLE 1
Characteristics of the Samples under Study

Sample	Crystal system	Unit cell parameters			Oxygen coefficient
		a	*b*	*c*	
PrBCO	O	3.912(3)	3.916(2)	11.751(3)	6.87
NdBCO	O[a]	3.894(2)	3.924(1)	11.777(3)	6.88
SmBCO	O	3.869(2)	3.915(1)	11.769(3)	6.87
EuBCO	O	3.862(2)	3.911(3)	11.740(3)	6.89
GdBCO	O	3.861(2)	3.913(2)	11.761(4)	6.85
DyBCO	O	3.840(2)	3.904(2)	11.723(4)	6.87
HoBCO	O	3.840(2)	3.899(1)	11.702(3)	6.8
ErBCO	O	3.826(1)	3.896(1)	11.687(3)	6.83
TmBCO	O	3.820(1)	3.893(1)	11.694(4)	6.85
YbBCO	O	3.812(1)	3.894(2)	11.681(3)	
Nd_2CuO_4	T	3.948(0)		12.184(1)	4.00
$Nd_{1.95}Ce_{0.05}CuO_4$	T	3.951(0)		12.167(2)	4.00
$Nd_{1.90}Ce_{0.10}CuO_4$	T	3.951(0)		12.125(3)	4.00
$Nd_{1.85}Ce_{0.15}CuO_4$	T	3.951(0)		12.095(1)	4.00
$Nd_{1.80}Ce_{0.20}CuO_4$	T	3.952(0)		12.069(1)	4.00

Note. O, orthorhombic; T, tetragonal.
[a] $BaCuO_2$ impurity 12%.

Oxygen content in RBCO materials has been determined by iodometry, according to literature data. The obtained results have been checked with the experimental measure of the lattice parameter and found in agreement (13).

The FT-IR spectra have been recorded using a Nicolet Magna 750 Fourier transform instrument. For the region 4000–350 cm^{-1} a KBr beam splitter has been used with a DTGS detector, while for the FIR region (600–50 cm^{-1}) a "solid substrate" beam splitter and a DTGS polyethylene detector have been used. KBr pressed disks (IR region) or polyethylene pressed disks and samples deposed on Si disks (FIR region) were used.

3. RESULTS AND DISCUSSION

a. XRD Characterization of Cuprate Phases

XRD data with the experimental lattice parameters and oxygen content of all samples are summarized in Table 1.

The 214 series compounds $Nd_{2-x}Ce_xCuO_4$ are crystallized in the so-called *T'* tetragonal structure of Nd_2CuO_4 and they are all monophasic without any detectable impurity. The lattice parameter *a* is unaffected by Ce content, while *c* strongly depends on cerium substitution, following the linear Vegard's law, in agreement with previous data (14). Oxygen content is easily stabilized at the stoichiometric amount, in this case.

All samples belonging to the 123 RBCO-type phase are crystallized in the orthorhombic structure, with the anomaly of the PrBCO sample which presents a very small orthorhombic distortion. In fact the lattice parameters *a* and *b* are almost coinciding, as in the tetragonal structure. NdBCO shows also the presence of $BaCuO_2$ phase as an impurity in an amount of about 12%. The lattice parameters of the RBCO compounds decrease at the increasing of the atomic number of the rare earth, because of the lowering of their ionic radius.

b. Description of the Structures, Theoretical Background, and Empirical Assignment of Vibrational Modes

$Nd_{2-x}Ce_xCuO_4$ compounds with $x \leq 0.25$ have the same tetragonal body-centered structure of Nd_2CuO_4, belonging to the $I4/mmm = D_{4h}^{17}$ space group with $Z = 2$ (15). In the primitive cell, only one molecular unit is present. This is the so-called *T'* structure, constituted by single sheets of square-planar coordinated copper ions and of linearly bicoordinated oxide ions with stoichiometry $[CuO_2]_n$ (Cu–O distance 1.97 Å (15)) separated by blocks with stoichiometry $[Nd_2O_2]_n$. Two types of oxygen ions exist: O(I), located in the superconducting planes, are coordinated linearly to two copper ions but also to four Nd(Ce) ions; O(II), located in the $[Nd_2O_2]_n$ blocks, coordinates only four Nd ions with a nearly tetrahedral geometry. The overall Nd coordination is eight (square-based prismatic) with four shorter Nd–O distances (2.3 Å with O(II)) and four longer Nd–O distances (2.7 Å with O(I)).

The factor group analysis (16) gives the irreducible representation reported in Table 2, in agreement with previous studies (5, 17). We can attempt an interpretation of

TABLE 2
Interpretation of the Vibrational Structure of Tetragonal Nd_2CuO_4, Orthorhombic $RBa_2Cu_3O_7$, and Tetragonal $RBa_2Cu_3O_6$

Sym.	Activity	Total	Acoustical	Optical	CuO_2 sheets	Nd_2O_2 blocks	CuO_3 chains		CuO_2 "molecules"		Cu–O apical str.	Lattice
					Internal	Internal	Int.	Libr.	Int.	Libr.		
					Nd_2CuO_4							
A_{1g}	R	1	0	1	0	1						0
B_{1g}	R	1	0	1	0	1						0
E_g	R	2	0	2	0	2						0
A_{2u}	IR	4	1	3	1	1						1
B_{2u}	ia	1	0	1	1	0						0
E_u	IR	5	1	4	2	1						1
					$RBa_2Cu_3O_7$							
A_g	R	5	0	5	2		1	0			1	1
B_{2g}	R	5	0	5	2		0	1			0	2
B_{3g}	R	5	0	5	2		1	0			0	2
B_{1u}	IR	8	1	7	2		2	0			1	2
B_{2u}	IR	8	1	7	2		2	0			0	3
B_{3u}	IR	8	1	7	2		2	0			0	3
					$RBa_2Cu_3O_6$							
A_{1g}	R	4	0	4	1				1	0	1	1
B_{1g}	R	1	0	1	1				0	0	0	0
E_g	R	5	0	5	2				0	1	0	2
A_{2u}	IR	6	1	5	1				1	0	1	2
B_{2u}	ia	1	0	1	1				0	0	0	0
E_u	IR	7	1	6	2				1	0	0	3

Note. ia, inactive mode.

the vibrational structure of these solids with a separation of the "internal" vibrations of the $[CuO_2]_n$ sheets, the internal vibrations of the $[Nd_2O_2]_n$ blocks, and the lattice vibrations of these two units (Table 2).

Of the internal modes of the $[CuO_2]_n$ sheets two are in-plane degenerate modes (E_u) and two are out-of-plane modes, with atom displacements parallel to the c axis (A_{2_u} and B_{2_u}). The IR active in-plane modes have the mixed character of asymmetric Cu–O–Cu stretching and of in-plane Cu–O–Cu deformation, with the predominance of one or the other in the two modes. The two IR out-of-plane modes are two different out-of-plane deformations of the $[CuO_2]_n$ sheets, one of them being IR active (A_{2_u}) and the other inactive (B_{2_u}). So, the internal vibrations of the superconducting sheets in this T' structure do not give rise to any Raman active mode. This indicates that IR spectroscopy should be more informative than Raman spectroscopy in this case, in spite of the more frequent use of the latter technique.

The internal vibrations of the $[Nd_2O_2]_n$ give rise to two IR active modes that have both the character of mixed stretching and deformations of Nd–O(II) bonds. The two lattice modes, both IR active, correspond to movements of the superconducting layers against the Nd–O blocks (A_{2u}) that have the character of symmetric Nd–O(I) stretchings and to sliding of the Cu–O(I) layers with respect to Nd–O(II) blocks (E_u).

A comparison of the results of this simplified approach based on the so-called group approximation with those of the lattice dynamics calculations performed, e.g., by Heyen *et al.* (17) shows that they do not disagree. Accordingly, seven IR active modes are expected for the whole structure, three of which are associated with internal vibrations of Cu–O sheets, two with those of Nd–O(II) blocks, and two with lattice vibrations (sheets against blocks).

In Table 3 the bands observed in our powder spectra are compared with the TO and LO single crystal modes reported by Heyen *et al.* (17), with the corresponding approximate description. We must mention that their powder spectra are also affected by powder morphology (18), so that the positions of the observed bands do not correspond to the TO modes but are more or less shifted toward the LO modes, as can be observed in Table 3.

$RBa_2Cu_3O_{7-y}$ compounds ($y < 0.5$) belong to the orthorhombic space group $Pmmm = D^1_{2h}$ with $Z = 1$ (19). The stoichiometric $RBa_2Cu_3O_7$ structure is based on two sheets of square planar copper and bicoordinated oxygen

TABLE 3
Position of the Observed IR Bands (cm^{-1}) and Approximate Assignments for $Nd_{2-x}Ce_xCuO_4$ Compounds

Sym.	TO (Ref. 17)	LO	Powder $X = 0$ (This work)	0.05	0.10	0.15	0.20	Approx. assignment
				593	593	593	590	Defect due to Ce
E_u	512	593	518	514	511	513	510	νCu–O(I)
A_{2u}	516	559	525	525	525	525	525	Nd–O(II)
E_u	353	432	380	380	380	(380)	(380)	Nd–O(II)
E_u	304	341	(320)					δ_{ip}Cu–O(I)
A_{2u}	282	433	312	309	318	319	309	δ_{oop}Cu–O(I)
A_{2u}	134	144	141					Lattice (Nd–O(I))
E_u	132	139	131	138	138	137	136	Lattice (slide)

atoms $[CuO_2]_n$ separated by eightfold coordinated R ions. The CuO_4 units are not squares and not exactly planar, with Cu–O distances near 1.93 along the x axis and 1.96 Å along the y axis as an effect of the orthorhombic distortion. These two planes, considered responsible for superconductivity, are intercalated by blocks constituted by $[CuO_3]_m$ chains disposed along the y axis and separated from each other by tenfold coordinated Ba ions. These chains contain Cu–O–Cu infinite sequences along the y axis at Cu–O distance 1.94 Å and two terminal oxygens per copper ion with short Cu–O bonds (1.84 Å) along the z axis. These terminal oxygens act as "apical" oxygens completing the square-pyramidal coordination of the Cu ions of the $[CuO_2]_n$ sheets, but with a much longer Cu–O bond (2.31 Å).

The factor group analysis (16) gives the irreducible representation given in Table 2, according to the literature (4, 5). These solids can lose oxygen. This occurs at the expense of the bridging linear oxygens of the $[CuO_3]_n$ chains that are interrupted and gives rise to isolated linear O–Cu–O groups along the z axis. When y becomes > 0.5, the structure converts from orthorhombic and metallic to tetragonal and semiconducting, and the superconducting transition is strongly displaced to lower T_c. This transition occurs progressively at y near 0.5 with the intermediacy of an orthorhombic superstructure (orthoII). The y value at which these transitions occur also depends on the rare earth ion R. When $y = 1$ (i.e., all bridging oxygen atoms in the chains are lost), the stoichiometric semiconducting phase $RBa_2Cu_3O_6$ is obtained, tetragonal, belonging to the space group $P4/mmm = D^1_{4h}$, with $Z = 1$ (19). In this case the Cu–O distances in the sheets all become equivalent (1.94 Å), the Cu–O distance in the isolated O–Cu–O units becomes even shorter (1.81 Å), and the "apical" distance becomes longer (2.46 Å).

The factor group analysis of tetragonal $RBa_2Cu_3O_6$ gives the irreducible representation reported in Table 2. To attempt a comparison of the observed spectra of the different cuprate structures, we can separate the vibrational structure of the whole cell into those of the elements that compose it, i.e., CuO_2 sheets, CuO_3 chains, and Y and Ba ions. In both RBCO structures, two $[CuO_2]_n$ sheets are present, separated by R ions, in contrast to the NCCO structure where these sheets are single. Consequently, the vibrational modes of the two planar units in the RBCO structure couple, and so each shifts into two components, one symmetric and one antisymmetric with respect to the inversion center. So, twelve vibrational degrees of freedom are expected for these sheets in RBCO compounds, compared to six for the T' structure of Nd_2CuO_4. Moreover, in the case of orthorhombic RBCO compounds the CuO_4 squares convert into rectangles, due to orthorhombic distortion, and so a further splitting of the in-plane doubly degenerate modes occurs. In Table 4 the correlation of the internal modes of the $[CuO_2]_n$ sheets in the three structures is reported.

In the case of the $RBa_2Cu_3O_7$ structure, $[CuO_3]_n$ chains are also present. They are constituted by Cu–O–Cu–O infinite chains that are responsible for one asymmetric stretching (B_{2u}), one in-plane deformation (B_{1u}), and one out-of-plane deformation (B_{3u}). Moreover, O–Cu–O linear units with two terminal short Cu–O bonds perpendicular to Cu–O–Cu–O chains are present. They are responsible for one symmetric stretching (A_{1g}), one asymmetric stretching (B_{1u}), two in-plane deformations (B_{3g} and B_{2u}), and one out-of-plane deformation (B_{3u}). These CuO_3 infinite chains are also responsible for one librational mode (B_{2g}).

In the case of tetragonal $RBa_2Cu_3O_6$ the chains no longer exist (because bridging oxygens are lost), but O–Cu–O linear "molecules" are present. These molecules are responsible for one asymmetric stretching (A_{2u}), one symmetric stretching (A_{1g}), and one degenerate deformation (E_u). Moreover, these "molecules" are responsi-

TABLE 4
Correlation of Internal Vibrational Modes of $[CuO_2]_n$ Sheets in Different Cuprate Structures

Ass. F.G. →	$Nd_{2-x}Ce_xCuO_4$ D_{4h} (Ref. 17)			$YBa_2Cu_3O_6$ D_{4h} (Ref. 29)			$YBa_2Cu_3O_6$ D_{2h} (Ref. 25)		
νCu–O	E_u	(IR)	512	E_g	(R)	577	B_{2g}	(R)	579
							B_{3g}	(R)	526
				E_u	(IR)	502	B_{2u}	(IR)	546[a]
							B_{3u}	(IR)	565[a]
δ_{ip}CuO	E_u	(IR)	304	E_g	(R)	488	B_{2g}	(R)	370
							B_{3g}	(R)	n.d.
				E_u	(IR)	276	B_{2u}	(IR)	573[a]
							B_{3u}	(IR)	153[a]
δ_{oop}CuO(iph)	A_{2u}	(IR)	282	A_{1g}	(R)	401	A_g	(R)	440
				A_{2u}	(IR)	390	B_{1u}	(IR)	309
δ_{oop}CuO(oph)	B_{2u}	(ia)	(289)	B_{1g}	(R)	352	A_g	(R)	340
				B_{2u}	(IR)	n.d.	B_{1u}	(IR)	(308)[b]

Note. F.G., factor group; iph, the oxygens mouve in phase; oph, the oxygens move out of phase; n.d., not detected.

[a] Calculated values for IR active modes parallel to the conducting planes (non detectable).

[b] Calculated value for an IR active mode perpendicular to the conducting planes, not detected but detectable (in principle).

ble for one degenerate librational mode (E_g). In Table 5 the correlations of the vibrational modes of $[CuO_3]_n$ chains of $RBa_2Cu_3O_7$ and of O–Cu–O isolated "molecules" of $RBa_2Cu_3O_6$ are reported.

In Tables 4 and 5 the positions of the fundamental TO modes, taken from literature monocrystal studies, are reported. The assignment to the approximately described vibrational modes of our model agrees (or at least does not disagree) with the predominant atomic motions calculated by the authors of these references for the modes of corresponding symmetry. However, some of the frequency values reported in these papers are experimental and others are calculated. Some calculated fundamental frequencies and some assignments reported in these pa-

TABLE 5
Tentative Assignment of the Vibrational Modes of the $[CuO_3]_n$ Chains of $RBa_2Cu_3O_7$ Phases

Structure	Mode descr.	$YBa_2Cu_3O_6$ Sym.	Act.		$YBa_2Cu_3O_7$ Sym.	Act.	TO exp (Ref. 25)	LO	TO Calc[a]
Cu–O–Cu	Asym. str.				B_{2u}	IR	348	[b,c]	339
Linear chains	In-plane def.				B_{1u}	IR	280	290	348
	Out-of-pl. def.				B_{3u}	IR	354	[b,c]	218
	Asym. str.	A_{2u}	IR	—	B_{1u}	IR	563	588	588
O–Cu–O units	Sym. str.	A_{1g}	R	—	A_g	R	500		548
(Short	In-plane def.				B_{2g}	R	210		352
CuO bonds)	In-plane def.				B_{2u}	IR	362	[b,c]	452
	Out-of-pl. def.	E_u	IR	—	B_{3u}	IR	381	[b,c]	294
Libration		E_g	R	----	B_{3g}	R	303		293
Cu–O apical	Sym. str.	A_{1g}	R	—	A_g	R	154		183
	Asym. str.	A_{2u}	IR	—	B_{1u}	IR	191	208	171

[a] Calculated values.

[b] Calculated values of IR active modes parallel to the conducting planes (nondetectable).

[c] The correspondence between the eigenvectors calculated by Humlichek *et al.* (25) and our empirical assignment is not clear, likely due to the strong coupling of these modes.

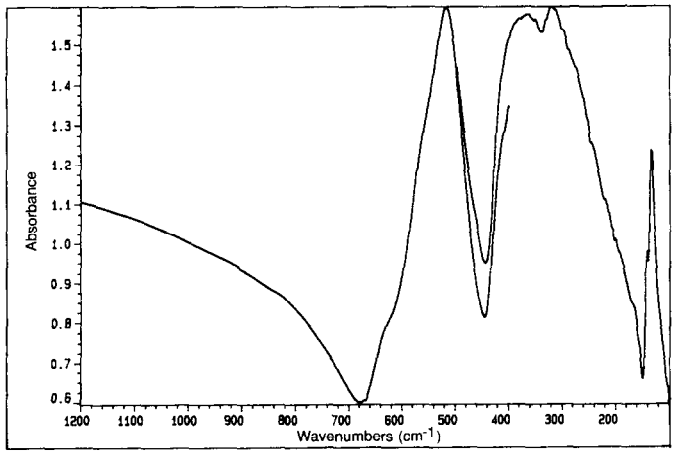

FIG. 1. FT-IR/FT-FIR spectrum of Nd_2CuO_4.

pers appear to be questionable on the basis of this correlation and of the below discussion.

c. FT-IR Spectra of Cuprate Powders

The IR spectrum of the pure Nd_2CuO_4 powder (Fig. 1) is characterized by a sharp strong band centered at 525 cm^{-1}, by a broader complex absorption in the region 420–250 cm^{-1} with two maxima at 380 and 310 cm^{-1}, and by a third sharp peak centered near 131 cm^{-1} with a clear shoulder at 140 cm^{-1}. The highest frequency band presents some morphological components at its higher frequency side. In Table 3 the bands observed in our powder spectrum are compared with the TO and LO crystal single modes reported by Heyen *et al.* (17), with the corresponding approximate description. The agreement of our data with those of Heyen *et al.* (17) seems to be quite satisfactory. The detection of five components observed by us agrees with the forecast of seven IR active modes because of the superimposition of two couples of modes.

The spectra of the samples belonging to the $Nd_{2-x}Ce_xCuO_4$ system (Fig. 2) are definitely similar to those of the parent compound Nd_2CuO_4 with few differences. The highest frequency band of Nd_2CuO_4 interpreted as due to the superimposition of two components, definitely splits as far as x increases. Moreover, what is even more evident, a rather sharp peak not observed for pure Nd_2CuO_4 grows at the higher frequency side of this band, near 590 cm^{-1} with increasing Ce addition. This peak corresponds to a Raman peak reported by several authors (17, 20, 21) to grow with increasing Ce content, just observed near 590 cm^{-1}, with apparent A_{1g} symmetry. However, to our knowledge, this peak was not reported previously in IR studies. More recent Raman studies suggested that this peak is also present, although weak, in the Raman spectrum of pure Nd_2CuO_4 and of some isostructural compounds and should be associated with a symmetry-forbidden mode made active by distortion of oxygen atoms along the CuO_2 plane (22). According to Table 3, the two IR active modes giving rise to the band near 520 cm^{-1} are stretchings of Cu–O planes and Nd–O blocks. Assuming that Ce ions substitute Nd^{3+} in the form of Ce^{4+}, justifying also the decrease of the c lattice parameter (Table 1), stronger Ce^{4+}–O^{2-} bonds should substitute weaker Nd^{3+}–O^{2-} bonds. So the stretchings of these new Ce^{4+}–O^{2-} "defective" bonds can be responsible for the new band at 590 cm^{-1}. The detection in both IR and Raman of this band could be associated with the loss of centrosymmetry of the unit cell where Ce ions are present and the consequent activation of the IR active Nd(Ce–O) mode also in Raman.

Other effects of Ce addition are (i) the slight shift down of the Cu–O band from 520 to 510 cm^{-1}; (ii) the progressive decrease in intensity of the bands near 520 cm^{-1} and of the shoulder near 380 cm^{-1}; and (iii) the progressive loss of resolution of the spectrum, finally substituted by a broad absorption centered near 300 cm^{-1}. These effects can be tentatively interpreted considering that for each Ce ion substituting Nd in the Nd–O blocks, one Cu^{2+} should be converted into Cu^{+} or, better, one electron should be added to the copper electron band. This tends to decrease the Cu–O bond order and, consequently, to decrease the Cu–O stretching frequency. This can justify the shift of the band near 520 cm^{-1} down to near 510 cm^{-1}, assigned to Cu–O stretching modes. This shift is very weak and the spectrum converts into a single broad band because of the delocalized nature of this electron and the consequent increased electron conduction of the materials toward the metallic one (23).

The other two most intense maxima near 140 and 320 cm^{-1} appear to have a more complex behavior, with a

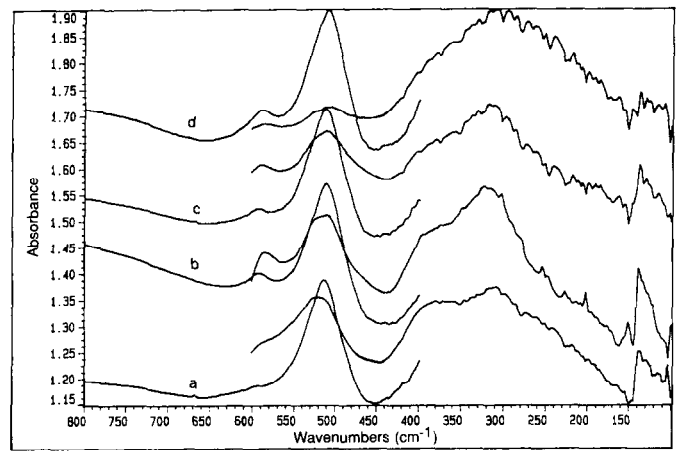

FIG. 2 FT-IR/FT-FIR spectra of $Nd_{2-x}Ce_xCuO_4$ solid solutions: (a) $x = 0.05$, (b) $x = 0.10$, (c) $x = 0.15$, and (d) $x = 0.20$.

FIG. 3 FT-IR/FT-FIR spectrum of $PrBa_2Cu_3O_{7-y}$.

maximum frequency for intermediate values of x, while the shoulder near 370 cm^{-1} seems to decrease in intensity with increasing x, perhaps because of a shift down that causes its loss of resolution with respect to the maximum near 310 cm^{-1}. It is tempting to relate this trend to the trend of T_c in these materials, which also shows a maximum for intermediate values of x. A reason for this can be associated with the instability of the planar fourfold coordination in the case of Cu^+, so that only a limited amount of additional electrons can be accommodated on the $[CuO_2]_n$ planes without substantial distortion.

The spectra of all RBCO compounds except PrBCO (Fig. 3) are composed only by a very broad absorption with few resolved components. The only well-resolved spectrum in the entire IR–FIR region is that of PrBCO (Fig. 4), and this is certainly related to the much lower electron conductivity of this semiconducting compound

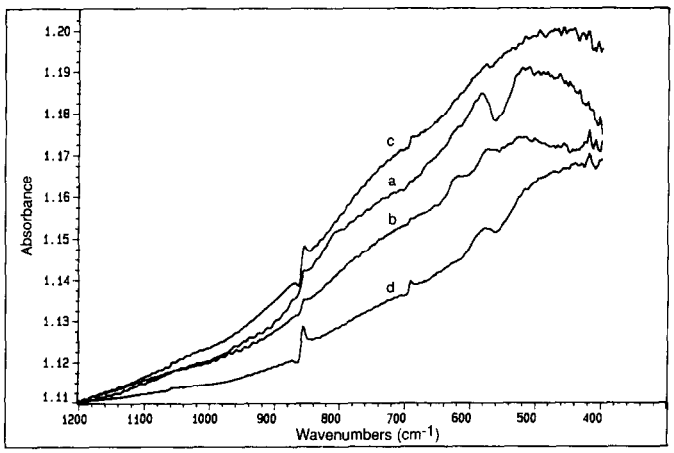

FIG. 4. FT-IR/FT-FIR spectra of (a) $YBa_2Cu_3O_{7-y}$, (b) $SmBa_2Cu_3O_{7-y}$, (c) $HoBa_2Cu_3O_{7-y}$, and (d) $TmBa_2Cu_3O_{7-y}$.

with respect to others of the series that are almost metallic (24).

As discussed above, 21 IR active modes are expected for these compounds. However, only five of them have been identified without uncertainty in the case of $YBa_2Cu_3O_{7-y}$, at 152 ± 3 cm^{-1}, 191 ± 8 cm^{-1}, 277 ± 7 cm^{-1}, 312 ± 6 cm^{-1}, and 565 ± 14 cm^{-1} (4). These bands have been assigned to five of the seven B_{1u} symmetry modes, one of which is assumed to be too weak to be detected and another of which is reported only by some authors to be located at 104 cm^{-1} (25). These modes are perpendicular to the CuO_2 conducting planes. Parallel modes (B_{2u} and B_{3u}) are considered to be screened out in metallic orthorhombic RBCO phases, according to the strongly anisotropic conductivity in these materials (25).

In the case of the semiconducting orthorhombic phase PrBCO, all 21 IR active modes should be observed. However, incomplete data are reported in the literature about the IR spectrum of PrBCO. In particular, some scattered data are reported for powders (7, 26) and one paper gives the position of 14 IR active TO modes for PrBCO single crystals (25). Also in this case, five of the seven B_{1u} TO modes are experimentally observed, and their position is relatively near the peaks observed in the YBCO spectra. Additionally, four B_{2u} TO modes and five B_{3u} TO modes were observed. The positions of the corresponding LO modes and of all other fundamental modes have been calculated by the authors of Ref. (25).

The position of the IR bands we observed in our powder spectra is compared with that of the fundamental TO bands as experimentally observed in orthorhombic PrBCO single crystals (25) and in orthorhombic YBCO powders and single crystals (4, 25, 27). The agreement between our data for PrBCO and the data reported by Humlicek *et al.* (25) is quite good. However, at least one more component is observed in our spectrum at 622 cm^{-1}. The spectra of all the other orthorhombic RBCO phases show two evident vibrational features near 620 and 570 cm^{-1}. The last feature, not very sensitive to the substitution of the trivalent element, can be assigned, on the basis of Table 5, to the asymmetric stretching of the CuO_2 short bonds in $[CuO_3]_n$ chains. This band is observed, in the case of PrBCO, at higher frequency than the other *R*BCO compounds (Table 5). This can be associated with the c lattice parameter for PrBCO being higher than for isostructural compounds; this probably allows a lower interaction from "apical" oxygens and Cu(I), allowing a strengthening of the bond of these oxygens with Cu(II) and, as consequence, a further shortening of the shortest Cu–O bonds.

Studies on the effect of the quenching temperature and oxygen content on the IR spectra of RBCO materials

TABLE 6
Experimentally Observed IR Active Modes for Orthorhombic *R*BCO Phases

YBCO s.c. (Ref. 25)		PrBCO s.c. (Ref. 25)				
TO	LO	TO	LO (calc.)	Sym.	PrBCO powder (This work)	Approx. description
					622	As. str. O–Cu–O units (O-def.)
563	588	590		B_{1u}	580	As. str. O–Cu–O units (O-sat.)
		552		B_{3u}	554	As. str. CuO_2 sheets
				B_{2u}	540	As. str. CuO_2 sheets
		373	544	B_{3u}	(410)	δ_{ipl} O–Cu–O units
		358	369	B_{2u}	(370)	δ_{opl} O–Cu–O units
						As str. Cu–O chains
309	348	340	478	B_{1u}	395	δ_{opl} CuO_2 sheets in phase
		280	315	B_{3u}	285	δ_{ipl} CuO_2 sheets
		271	275	B_{2u}	275	δ_{ipl} CuO_2 sheets
280	290	267	270	B_{1u}	250	Lattice
191	208	196	208	B_{1u}	202	As. str. Cu–O apical
		192	202	B_{3u}		
		171	186	B_{2u}		
151	186	163	175	B_{1u}	169	Lattice
		150	161	B_{3u}	155	
		127	131	B_{2u}	132	

Note. O-def., oxygen deficient structure; O-sat., oxygen saturated structure.

showed that a band near 640 cm^{-1} observed in tetragonal $YBa_2Cu_3O_{7-y}$ ($y = 0.5$) progressively disappeared with decreasing y (4, 28). This band, which was not included in the lattice dynamics calculations for $YBa_2Cu_3O_6$ by Thomsen *et al.* (29), is very likely associated with the asymmetric stretching of the O–Cu–O "molecules" in $YBa_2Cu_3O_6$-like structure. In fact these bonds are significantly shorter in $YBa_2Cu_3O_6$ with respect to $YBa_2Cu_3O_7$ and should give rise to stretching modes at significantly higher frequencies. The copresence of bands near 620–640 cm^{-1} and near 570 cm^{-1} in RBCO phases with $0 \leq x \leq 0.5$ is probably indicative of the copresence of CuO_2 molecules in $YBa_2Cu_3O_6$-like structures and of $[CuO_3]_n$ chains in $YBa_2Cu_3O_7$-like structures, respectively, that are now known to be partly ordered (30, 31). If this hypothesis is correct, the intensity of the feature in the 640–600 cm^{-1} region should allow one to monitor the oxygen content in the samples.

The comparison of the spectra observed for Nd_2CuO_4 and for $PrBa_2Cu_3O_{7-y}$ and isostructural compounds and their interpretation, given in Tables 3 and 6, also indicate that the bands associated with the modes of CuO_2 sheets are observed at lower frequencies in the former than in the latter. This can be associated to the longer Cu–O distance in the former than in the latter case. In effect, at least for stretching modes a rough inverse correlation between Cu–O distance and observed frequency can be deduced from these data as expected.

4. CONCLUSIONS

The conclusions of this work can be summarized as follows:

(i) The vibrational skeletal spectra of different cuprate structures can be discussed comparatively on the basis of the interpretation of the vibrational structure proposed above, based on group approximation.

(ii) Semiconducting materials like Nd_2CuO_4 and $PrBa_2Cu_3O_{6.8}$ give rise to well-resolved powder IR–FIR spectra while metal-like materials like $Nd_{1.8}Ce_{0.2}CuO_4$ and $YBa_2Cu_3O_{6.8}$ give rise to spectra dominated by a broad band in the region below 500 cm^{-1}, associated with metallic conduction.

(iii) Doping of Nd_2CuO_4 with Ce causes the formation of a new band, observed in both IR and Raman spectra near 590 cm^{-1}, tentatively assigned to an IR active Nd(-Ce)–O stretching mode activated in Raman, too, due to a strong distortion of the centrosymmetric T' structure. Simultaneously, other spectral modifications are observed that can be interpreted as evidence of the increase of the electron densities in the copper band and a progressive distortion of Cu–O sheets.

(iv) The IR active Cu–O stretching modes are inversely well correlated with the Cu–O distances. So, for the Cu–O sheets they fall at lower frequency for NCCO than RBCO compounds.

(v) The higher frequency Cu–O stretching modes in

$RBa_2Cu_3O_7$ materials (580 cm^{-1}) are associated with the asymmetric stretching of O–Cu–O terminal units along the c axis. The presence of components near 620 cm^{-1} is indicative of oxygen deficient structures like in $RBa_2Cu_3O_6$. Consequently the intensity of these features is indicative of the oxygen content in the sample.

ACKNOWLEDGMENTS

This work has been supported by MURST. We are thankful to Prof. G. L. Olcese for helpful suggestions and discussions.

REFERENCES

1. J. G. Bednorz, and K. A. Muller, *Z. Phys. B. Condens. Matter* **64,** 189 (1986).
2. H. Muller-Buschbaum, *Angew. Chem. Int. Ed. Engl.* **28,** 1472 (1989).
3. J. B. Goodenough, and A. Manthiram, *in* "Studies of High Temperature Superconductors" (A. Narlikar, Ed.), Vol. 5, p. 1. Nova, New York, 1990.
4. R. Feile, *Physica C* **159,** 1 (1989).
5. C. Thomsen, *in* "Light Scattering in Solids VI" (M. Cardona, and G. Güntherodt, Eds.), Topics in Applied Physics, Vol. 68, p. 285. Springer–Verlag, Heidelberg, 1991.
6. M. Cardona, *J. Phys. Chem. Solids* **54,** 1287 (1993).
7. S. Onari, A. Ono, T. Arai, and T. Mori, *Physica B* **165–166,** 1235 (1990).
8. G. A. Costa, M. Ferretti, M. L. Fornasini, and G. L. Olcese, *Solid State Commun.* **65** 469 (1988).
9. M. M. Carnasciali, G. A. Costa, M. Ferretti, and E. A. Franceschi, *J. Therm. Anal.* **37,** 1709 (1991).
10. G. Busca, G. Ricchiardi, D. Siew Hew Sam, and J. C. Volta, *J. Chem. Soc. Faraday Trans.* **90,** 1161 (1994).
11. M. I. Baraton, G. Busca, M. C. Prieto, G. Ricchiardi, and V. Sanchez Escribano, *J. Solid State Chem.* **112,** 9 (1994).
12. M. Daturi, M. Ferretti, and E. A. Franceschi, *Physica C* **347,** 235–240, (1994).
13. P. Lanza, and G. Rossi, *Anal. Chim. Acta.* **244,** 253 (1991).
14. T. C. Huang, E. Moran, A. I. Nozzal, J. B. Torrance, and P. W. Wang, *Physica C* **159** 625 (1989).
15. H. K. Muller-Buschbaum, and W. Wollschlager, *Z. Anorg. Allg. Chem.* **414,** 76 (1985).
16. W. G. Fateley, F. R. Dollish, N. T. McDevitt, and F. F. Bentley, "Infrared and Raman Selection Rules for Molecular and Lattice Vibrations: The Correlation Method." Wiley, New York, 1972.
17. E. T. Heyen, G. Kliche, W. Kress, W. Konig, M. Cardona, E. Rampf, J. Prade, U. Schroder, A. D. Kulkarni, F. W. de Wette, S. Pinol, D. McK. Paul, E. Moran, and M. A. Alario Franco, *Solid State Commun.* **74,** 1299 (1990).
18. S. Hayashi, N. Nakamori, J. Hirono, and H. Kanamori, *J. Phys. Soc. Jpn.* **43,** 2006 (1977).
19. B. G. Hyde, and S. Andersson, "Inorganic Crystal Structures." Wiley, New York, 1989.
20. V. M. Orera, M. L. Sanjuan, R. Alcalà, J. Fontcuberta, and S. Pinol, *Physica C* **168,** 161 (1990).
21. W. Sadowski, H. Hagemann, M. Francois, H. Bill, M. Peter, E. Walker, and K. Yvon, *Physica C* **170,** 103 (1990).
22. M. Udagawa, Y. Nagaoka, N. Ogita, M. Masada, J. Akimitsu, and K. Ohbayashi, *Phys. Rev. B* **49,** 585 (1994).
23. Y. Tokura, H. Takagi, and S. Uchida, *Nature* **337,** 345 (1989).
24. E. M. Engler, V. Y. Lee, A. I. Nazzal, R. B. Beyers, G. Lim, P. M. Grant, S. S. P. Parkin, M. L. Ramirez, J. E. Vasquez, and R. J. Savoy, *J. Am. Chem. Soc.* **109,** 2848 (1987).
25. J. Humlicek, A. P. Litvinchuk, W. Kress, B. Lederle, C. Thomsen, M. Cardona, H. U. Habermeier, I. E. Trofimov, and W. Konig, *Physica C* **206,** 345 (1993).
26. J. Klamut, T. Glowiak, J. Hanuza, Z. Henkie, R. Horyn, B. Jezowska-Trzebiatowska, R. Kubiak, K. Lukaszewicz, J. Stepien-damm, and A. Zygmunt, *Physica C* **153–155,** 288 (1988).
27. M. Cardona, L. Genzel, R. Liu, A. Wittlin, H. Mattausch, F. Garcia Alvarado, and E. Garcia-Gonzalez, *Solid State Commun.* **64,** 727 (1987).
28. Y. Saito, H. Sawada, T. Iwazumi, Y. Abe, H. Ikeda, and R. Yoshizaki, *Solid State Commun.* **64,** 1047 (1987).
29. C. Thomsen, M. Cardona, W. Kress, R. Liu, L. Genzel, M. Bauer, E. Shonherr, and U. Schroder, *Solid State Commun.* **65,** 1139 (1988).
30. H. F. Poulsen, N. H. Andersen, J. V. Andersen, H. Bohr, and O. G. Mouritsen, *Nature* **349,** 594 (1991).
31. G. Cannelli, R. Cantelli, F. Cordero, F. Trequattrini, and M. Ferretti, *Solid State Commun.* **82,** No. 6, 433 (1992).